Microscopic structure of the NL10 heat-treatment center in silicon: Study by electron-nuclear double resonance

T. Gregorkiewicz,* H. H. P. Th. Bekman, and C. A. J. Ammerlaan
Natuurkundig Laboratorium der Universiteit van Amsterdam, Valckenierstraat 65, NL-1018 XE Amsterdam, The Netherlands
(Received 2 October 1987; revised manuscript received 18 March 1988)

The defect center giving rise to the Si-NL10 EPR spectrum has been investigated by the electron-nuclear double-resonance (ENDOR) technique. Three separate experiments have been performed: oxygen ENDOR of ^{17}O nuclei, aluminum ENDOR of ^{27}Al, and field-stepped ENDOR. As a result a microscopic model for the Si-NL10 center can be proposed. According to that model the Si-NL10 center is an oxygen cluster which may also incorporate an acceptor. The center grows during annealing at about 470 °C and develops several species by subsequent addition of oxygen atoms along a $[0\bar{1}1]$ direction. In the studied sample the basic Si-NL10 center species was of orthorhombic $2mm$ (C_{2v}) symmetry type and contained two oxygen atoms and an aluminum atom. More tentatively, we propose that a vacancy exists on the twofold axis of the defect. The next species to develop upon annealing had the symmetry lowered to monoclinic m type (C_{1h}) and contained most probably three oxygen atoms. The lowering of the symmetry cannot be resolved in EPR which retains the overall orthorhombic character. Oxygen atoms incorporated in the center take the usual puckered bonded interstitial position with the bond angle of about 114°. The structure of the Si-NL10 center is planar in the (011) plane, while at the same time that crystallographic plane appears as forbidden in regard to the spin distribution. On the basis of the constructed model, two possible interpretations of the Si-NL10 center are proposed; one of them identifies it as an acceptor [$(TD)^-$] state of the silicon thermal donor (TD).

I. INTRODUCTION

Shallow donor states are formed in oxygenrich silicon upon heat treatment in the 300–500 °C temperature range.[1–3] The defects giving rise to those states are generally termed thermal donor centers (TD's) and have been thoroughly studied over the past thirty-five years. However, the experimental data gathered is not well correlated and frequently contradicting.[4] Nevertheless it is generally accepted that centers of donor character are formed as a result of oxygen clustering, although the microscopic structure and growth mechanism of thermal donors remains unclear. The early work focused on the formation kinetics as determined from the resistivity measurements. Kaiser *et al.*[3] found an initial growth rate and a maximum concentration of thermal donors to be proportional, respectively, to a fourth and third power of the initial oxygen concentration. That led them to propose a Si_nO_4 complex as a first model for TD. More recently, however, it has been found that those simple power dependences are not generally followed, with the possible exception of boron-doped material.[5]

Information about the electronic structure of thermal donors was obtained from infrared measurements. Wruck and Gaworzewski[6] discovered two series of shallow donor levels connected to the neutral and singly ionized charge states of the double donor defect. Later studies[7] revealed a series of up to nine different double donors with slightly different ground-state energies. This result could not be understood within the model of Kaiser *et al.*

Important structural information on thermal donors was obtained from electron paramagnetic resonance (EPR) measurements.[8,9] These studies revealed a variety of heat-treatment centers, predominantly of $2mm$ (C_{2v}) point-group symmetry, which could be related to thermal donors on the basis of production characteristics. One of these centers, ("narrow-line") Si-NL8, could be identified with the singly ionized state of the double donors as found in the infrared absorption.[10] However it was not clear at this stage whether Si-NL8 was connected to one or more of the nine thermal donors. We will refer to these thermal donors hereafter as the NL8 thermal donor (NL8 TD), keeping open the possibility that other thermal donors, not necessarily connected to the Si-NL8 EPR spectrum, could also exist. The identification of Si-NL8 with the infrared double donors was possible due to the infrared and deep-level transient spectroscopy (DLTS) studies under uniaxial stress.[11–14] The infrared studies revealed that the ground-state wave function of the NL8 TD in its neutral and singly ionized charge state is effective-mass-like,[15] and could be constructed from a single pair of conduction-band valleys. Additional small splittings due to deviations from the effective-mass theory, show that the wave function of the NL8 TD is distorted by an extended "central cell" with $2mm$ symmetry (consistent with the point-group symmetry of the Si-NL8 EPR spectrum).

The new experimental data stimulated theoretical efforts and a number of alternative models has been pro-

posed: Ylid,[16] Ourmazd-Schröter-Bouret (OSB),[17] Si_i.[18] Among them the OSB model seemed most promising. According to this model the electrical activity commences with clusters containing five or more oxygen atoms, and arises from a divalent silicon atom at the center of the cluster. The donor activity of a cluster is terminated upon the ejection of this central silicon atom in order to release the stress accumulated by a gradual growth of the cluster. Calculations by Robertson and Ourmazd[19] estimated the hyperfine interaction with a central ^{29}Si atom to be about 80 MHz for the smallest thermal donor species. Unfortunately the recent electron-nuclear double-resonance (ENDOR) measurements performed on the Si-NL8 spectrum[20] failed to unravel such interaction, thus undermining the OSB model. The ^{29}Si ENDOR study revealed at least five different species and correlated them to five infrared double donors. It was clearly shown that the Si-NL8 spectrum was an average of several EPR spectra related to a series of NL8 TD's. Having contradicted the OSB model by the experiment, Michel *et al.*[20] proposed that the core of the NL8 TD consisted of a low-abundance nucleus, possibly an O_2 molecule. According to calculations of DeLeo *et al.*[21] a substitutional oxygen pair in silicon can have shallow-donor properties with electrical levels just below the conduction band when the two oxygen atoms are squeezed together. However an ^{17}O ENDOR experiment should be carried out to support this idea.

At the same time also other EPR active heat-treatment centers besides Si-NL8 seemed to be related to thermal donors. In that situation the aim of this research project was to study and reveal the microscopic structure of the heat-treatment centers by means of the electron-nuclear double-resonance technique.

II. PRELIMINARIES

Extensive electron paramagnetic resonance studies preceded the ENDOR experiments. The results of those studies have been published in advance[5,22] and are briefly summarized below.

The EPR investigations were performed on both Czochralski-grown and float-zoned (FZ) silicon diffused with natural and isotopically enriched oxygen. Since the majority of the existing experimental data concerned only boron-doped silicon (with the important exception of the work by Fuller *et al.*[23]) it was important to study the influence of other dopants. Following that objective, samples doped with aluminum, indium, gallium, and phosphorus were investigated in addition to boron-doped material. A new, ultraclean diffusion technique was developed by means of which high concentrations of the ^{17}O magnetic oxygen isotope could be introduced into silicon.

In the studies two different $2mm$-symmetry spectra were seen: Si-NL8 and Si-NL10 as labeled when first reported by Muller *et al.*[8,9] for heat-treated boron-doped Czochralski-grown Si. The EPR results were similar for Czochralski-grown and FZ oxygen-doped silicon regardless of the dopant present in the sample. The relative concentrations of the EPR centers ruled out the possibility of relating Si-NL8 to residual boron concentrations. The Si-NL8 spectrum could not be observed in phosphorus-doped silicon, which can possibly be understood as Si-NL8 is related to the singly ionized state of the NL8 TD;[10] in phosphorus-doped material the Fermi level is close to the phosphorus donor level and NL8 TD's are in the neutral, nonparamagnetic state. The studies have shown that the production of the Si-NL8 spectrum was favored in boron-doped material. The Si-NL10 spectrum which could be observed for all the investigated samples attained the highest concentration for aluminum doping. Following the results of the studies any hypothesis of direct acceptor involvement in the structure of heat-treatment centers became doubtful. However, the incorporation of the dopant could not be ruled out completely. If the dopant takes a position where the spin density is low for symmetry reasons, this might lead to undetectable changes in the EPR spectrum. A different dopant would then produce the same EPR spectrum.

Another characteristic feature of the Si-NL8 spectrum, the shifting of its g values with increased annealing time while preserving the $2mm$ symmetry, was confirmed.[9] The studies have further revealed that the Czochralski-grown Si samples, which had higher oxygen concentration, were always in a later stage of the g-shifting process than the FZ oxygen-doped material. A similar transformation process was discovered for the Si-NL10 spectrum. It is illustrated in Fig. 1 where the separation ΔB of the two resonances observed with the magnetic field **B** parallel to the [111] direction is plotted against the annealing time. This separation ΔB is proportional to component g_{yz} of the g tensor. It was found that the EPR spectra Si-NL10, Si-NL13, and Si-NL17 reported earlier by Muller *et al.*[8] correspond to different transformation stages of the same center. Also, as in the case of the Si-NL8, the same forward shift on the time scale of the g-value transformation for higher oxygen contents could be noted (Fig. 1).

For all the studied samples, as far as the available concentrations were concerned, the Si-NL10 centers presented the more likely candidates to account for the resistivity changes (as measured at room temperature by four-point probe). Since at the same time Si-NL8, and not the Si-NL10 center, had been correlated to the shallow double donor levels as found in the infrared,[10,20] we decided to further investigate the Si-NL10 center.

Here especially the incorporation of oxygen presented an intriguing question. The oxygen diffused samples with enriched concentration of the ^{17}O isotope were first carefully examined in the EPR measurements for any ^{17}O hyperfine structure. No such structure was observed. However an ENDOR attempt that followed was successful. In the preliminary ENDOR measurements of Si-NL10 the involvement of at least two oxygen nuclei in the structure of that center had unambiguously been established.[24] At the same time ENDOR resonances arising from interactions with ^{27}Al and ^{29}Si nuclei had also been observed.

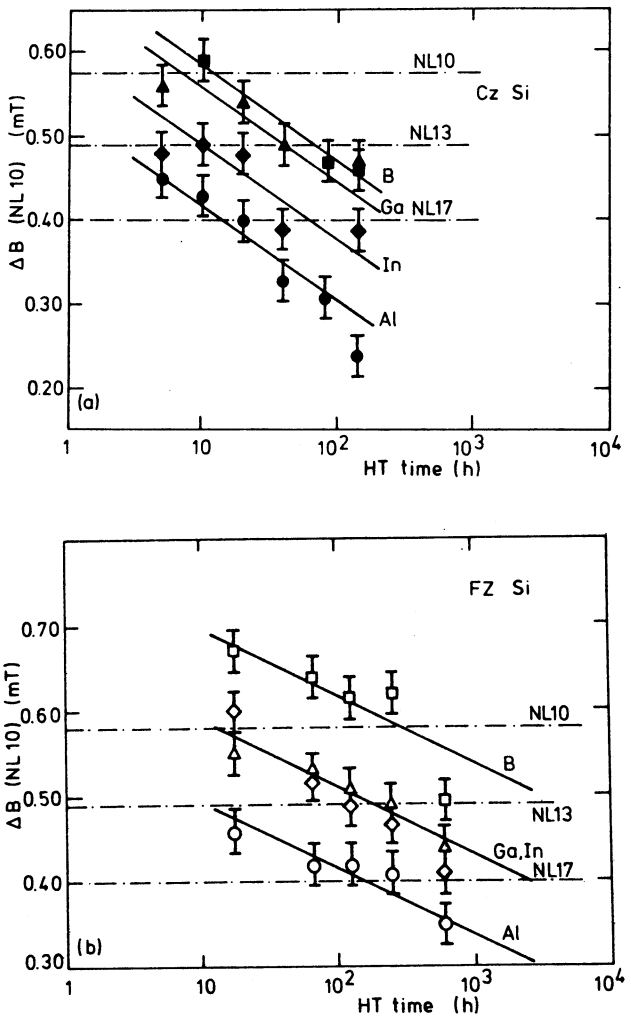

FIG. 1. The annealing time dependence of g-value shifting for the Si-NL10 spectrum as observed under (white light) illumination for (a) Czochralski-grown (Cz) and (b) float-zoned (FZ) oxygen-diffused samples. The transformation of the spectrum is expressed as the time-dependent change of the separation ΔB between the two resonances observed with external magnetic field $\mathbf{B}\|[111]$. ΔB values are scaled to 23 GHz microwave frequency.

III. EXPERIMENTAL PROCEDURE

A. Equipment

The measurements were performed with a superheterodyne spectrometer operating at 23 GHz and adjusted to detect the dispersion part of the EPR signal. The magnetic field, modulated at a frequency of 83 Hz, could be rotated in the $(0\bar{1}1)$ plane of the sample. A cylindrical TE_{011}-mode silver-coated epibond cavity was used. In the thin silver layer on the cylindrical side wall of the cavity a spiral groove was cut which could serve as an ENDOR coil. For ENDOR measurements the radio frequency was square-wave modulated at 3.3 Hz to allow double phase-sensitive detection of the signal. The sample was held at 4.2 K. The ENDOR measurements were performed under white light illumination. Light from a halogen source was transmitted to the sample by a quartz rod.

B. The sample

The sample used for the ENDOR measurements was commercial (Wacker Chemitronic) aluminum-doped FZ silicon with resistivity $\rho=\sim 2\ \Omega$ cm, aluminum concentration $[Al]=9\times10^{15}$ cm^{-3}, and carbon concentration $[C]\leq 5\times10^{15}$ cm^{-3}. It had dimensions of $2\times2\times15$ mm^3 with its longest side corresponding to the $[0\bar{1}1]$ direction. The sample was further diffused with oxygen in the ultraclean diffusion procedure as previously described.[5] The total oxygen concentration, measured by the infrared absorption in the 9 μm band, was 4×10^{17} cm^{-3}, and the concentration of the ^{17}O magnetic isotope was 1.2×10^{17} cm^{-3}.[25] After the diffusion process, the sample was heated up to 1380 °C for half an hour. This was followed by a rapid quench to room temperature. Finally the sample was given a heat treatment for 200 h at 470 °C. After 200 h the sample was on the brink of p to n-type conversion. The EPR spectrum showed a strong Si-NL10 signal with a concentration of EPR active centers of $\sim10^{16}$ cm^{-3}.

Additionally, for the ^{27}Al ENDOR measurements, Czochralski-grown, aluminum-doped silicon samples of similar resistivity and carbon concentrations were used. The interstitial oxygen concentration was in that case higher $\sim1.2\times10^{18}$ cm^{-3}.

IV. EXPERIMENTAL RESULTS

A. General

The Si-NL10 EPR spectrum can be described with the simple spin-Hamiltonian

$$\mathcal{H}=\mu_B\mathbf{B}\cdot\vec{\mathbf{g}}\cdot\mathbf{S}\ , \tag{1}$$

with spin $S=\frac{1}{2}$. The symmetry of the defect wave function is reflected directly by the symmetry of the $\vec{g}$ tensor which in this case is of the $2mm$ point group. There are six different orientations possible in the silicon lattice for such a defect. These have been labeled here *ab*, *ac*, *ad*, *bc*, *bd*, and *cd* following the convention used by Sprenger *et al.*[26] for the V^- center. Because the rotation of the magnetic field takes place in a $(0\bar{1}1)$ plane, at most four different EPR lines can be observed in the experiment. The characteristic angular dependence of the Si-NL10 spectrum (in one of its later transformation stages) labeled with the corresponding orientations is shown in Fig. 2. The principal values for the g tensor are $g_1=1.997\,99$, $g_2=1.999\,46$, and $g_3=1.999\,82$ (literature values of Si-NL17).

Wherever orientation dependent information is given in this paper we will refer to the orientation labeled *ad*. In Fig. 3 the cubic axis system x,y,z is depicted for defect orientation *ad*. Also the principal axes of the g tensor are shown. For this orientation the [100] direction is the twofold axis and the two mirror planes are the $(0\bar{1}1)$ and the (011) crystallographic planes.

When the interaction with only one magnetic nucleus is added, then one can generally expect that the symme-

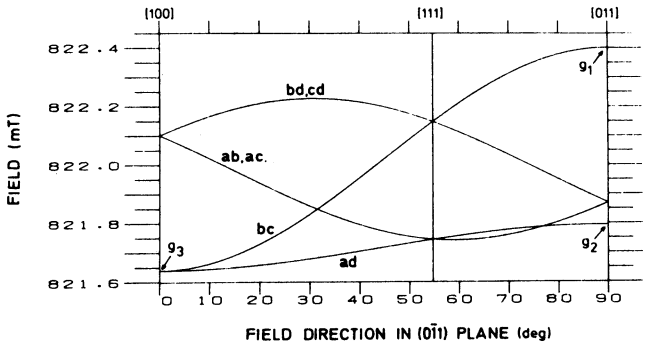

FIG. 2. The angular dependence of the Si-NL10 spectrum. The orientations are labeled in accordance with Sprenger *et al.*[26]

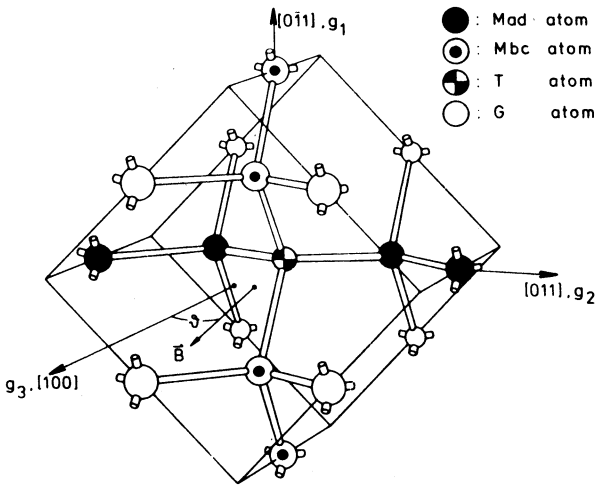

FIG. 3. The silicon lattice with the cubic axis system for defect orientation *ad* as used in the tables for the *A* and *Q* tensors. Also the principal directions of the *g* tensor are depicted, and the different types of atoms as can be discriminated in experiment.

try is lowered. The Hamiltonian can then be written as

$$\mathcal{H}=\mu_B \mathbf{B}\cdot\vec{\vec{g}}\cdot\mathbf{S}-g_N\mu_N\mathbf{B}\cdot\mathbf{I}+\mathbf{S}\cdot\vec{\vec{A}}\cdot\mathbf{I}\ . \tag{2}$$

The symmetry of the center together with the magnetic nucleus is now reflected in the symmetry of the $\vec{\vec{A}}$ tensor. In the most general case the magnetic nucleus takes a position somewhere around the defect and not on one of the perpendicular mirror planes. The resulting symmetry is then triclinic and yields a triclinic $\vec{\vec{A}}$ tensor of general class (*G* class). If the overall symmetry of the defect is 2*mm* there must be more magnetic nuclei involved in the defect. In the case when the nucleus is not lying on a mirror plane there have to be three other nuclei in positions symmetric with respect to the mirror planes. The four nuclei in the symmetry-equivalent positions form an ENDOR shell. In such a case one triclinic hyperfine (and quadrupole) tensor can be observed for the interaction with the four nuclei of one shell. In Fig. 3 the *G*-class atoms are indicated.

The symmetry of the center with an interacting nucleus can be higher than triclinic. When the nucleus is on a mirror plane the resulting symmetry is that of point group *m*. Here two atom positions are related by the symmetry operations of point group 2*mm*. In that case two different kinds of tensors are possible depending on the mirror plane involved; they will be called *Mad* and *Mbc* classes. The *Mad* and *Mbc* atoms are indicated in Fig. 3. Two *Mad* atoms symmetrical with respect to the (011) plane give rise to one *Mad* class hyperfine tensor (similar for *Mbc* atoms).

Finally it is also possible that the nucleus is lying on the twofold axis. There are no other symmetry related positions as the resulting symmetry is already 2*mm*. Those tensors will be called *T* class. A *T* atom is indicated in Fig. 3. Table I summarizes the properties of the four possible classes of interactions in 2*mm* symmetry.

In the ENDOR experiment it is possible to discriminate between the two mirror planes. For a magnetic field in the (0$\bar{1}$1) plane, the EPR resonances from interactions with atoms in positions symmetric with respect to this plane coincide resulting in double orientational degeneracies for defect orientations *ad* and *bc*. Therefore each of them gives two ENDOR lines for a general class tensor. In the case of the *m*-class symmetry orientation *ad* gives two lines and *bc* only one for an *Mad* class tensor; the situation is reversed for an *Mbc* tensor. Both *ad* and *bc* give only one ENDOR line for a 2*mm* tensor.

Although the Si-NL10 spectrum has a very small anisotropy, the EPR of orientations *ad* and *bc* are, for some ranges of angles, separated well enough to allow an unambiguous determination of the class for the observed ENDOR tensor.

For the interactions with nuclei with spin $I>\frac{1}{2}$ (as is the case for ^{17}O and ^{27}Al) the spin Hamiltonian given by Eq. (2) has to be supplemented with an extra term. This term describes the interaction with the quadrupole moment of the nuclei involved. The Hamiltonian becomes

TABLE I. Properties of the different types of hyperfine tensors and associated shells for a spectrum of 2*mm* symmetry like the Si-NL10. N_{at} is the number of atoms per shell and N_{el} is the number of independent tensor elements. The number of ENDOR lines is indicated for the three high-symmetry directions in the (0$\bar{1}$1) plane.

Class	Symmetry	N_{el}	N_{at}	Atom positions	No. of lines, B‖ [100]	[111]	[011]
T	2*mm*	3	1	[100] axis	2	2	3
Mad	*m*	4	2	(0$\bar{1}$1) plane	2	3	4
Mbc	*m*	4	2	(011) plane	2	3	4
G	1	6	4	others	3	4	6

then

$$\mathcal{H}=\mu_B \mathbf{B}\cdot\overleftrightarrow{g}\cdot\mathbf{S}-g_N\mu_N\mathbf{B}\cdot\mathbf{I}+\mathbf{S}\cdot\overleftrightarrow{A}\cdot\mathbf{I}+\mathbf{I}\cdot\overleftrightarrow{Q}\cdot\mathbf{I}\ . \tag{3}$$

From this Hamiltonian first-order solutions can be calculated, giving an overall view of the ENDOR patterns which can be expected in the experiment. These solutions are found as

$$E\mid m_S,m_I\rangle = m_S g_{\text{eff}}\mu_B B - m_I g_N\mu_N B + m_S m_I A_{\text{eff}} + m_I^2 Q_{\text{eff}}\ . \tag{4}$$

NMR transitions are determined by $\Delta m_S=0, \Delta m_I=\pm 1$. For the nuclear spin $I=\frac{5}{2}$ the NMR (or ENDOR) frequencies are

$$h\nu=\Delta E=\mid g_N\mu_N B \pm m_S A_{\text{eff}} \pm 4Q_{\text{eff}}\mid\ , \tag{5a}$$

$$h\nu=\Delta E=\mid g_N\mu_N B \pm m_S A_{\text{eff}} \pm 2Q_{\text{eff}}\mid\ , \tag{5b}$$

$$h\nu=\Delta E=\mid g_N\mu_N B \pm m_S A_{\text{eff}}\mid\ , \tag{5c}$$

where the $\pm$ signs before the effective A and Q values are unrelated.

EPR transitions are determined by $\Delta m_S=\pm 1, \Delta m_I=0$; the first-order solutions are

$$h\nu=\Delta E=g_{\text{eff}}\mu_B B + m_I A_{\text{eff}} \tag{6}$$

and there is no quadrupole contribution.

In the analysis of the experimental results the parameters of the spin Hamiltonian as given by Eq. (3) were fitted with the help of a Cyber 170 model 750 main-frame computer. The basic routines used were obtained from the International Mathematical and Statistical Library (IMSL). They allowed also to simulate the ENDOR spectra. This feature was found to be most helpful in analysis of the severely overlapping oxygen tensors.

B. ^{17}O ENDOR

Three different oxygen isotopes were present in the sample: ^{16}O, ^{17}O, and ^{18}O. However, only one of them, ^{17}O has a nuclear spin ($I=\frac{5}{2}$) and a quadrupole moment (Table II).

In our experiment the Zeeman frequency for the ^{17}O nucleus was around 4.7 MHz. In the [111] direction, where the tensors were separated most, the ^{17}O lines appeared up to a frequency of about 6.1 MHz. The full width at half maximum (FWHM) linewidth of the ENDOR resonances was $\sim$3 kHz; the small linewidth was crucial in discriminating between overlapping oxygen tensors.

From the measurements up to eight oxygen shells could be distinguished. It is remarkable that all the oxygen tensors were of the mirror plane class. Moreover, they were all of the same specific kind, namely, of the *Mbc* class. As a consequence one has to conclude that all the oxygen atoms in the Si-NL10 center are lying in the (011) plane for defect orientation *ad* (Fig. 3).

According to the literature[27] the $g_N\mu_N/h$ value for the ^{17}O nucleus is 5.772 MHz T^{-1}. It is however known that in solids the actual g_N value can deviate slightly from that number. Therefore in our computer analysis also the $g_N\mu_N/h$ value was fitted and found to be 5.774 MHz T^{-1}.

By inspecting both the ENDOR traces and the results of the computer fits, it turns out that all the tensors are very similar. The difference between the shells is mainly in the isotropic part of the hyperfine tensor. All the $\overleftrightarrow{A}$ tensors are almost isotropic and the quadrupole tensors $\overleftrightarrow{Q}$ are practically the same for all the shells. The absolute sign of a tensor cannot be determined from ENDOR measurements. Moreover the relative signs of the $\overleftrightarrow{A}$ and $\overleftrightarrow{Q}$ tensors cannot be determined either. Therefore for all hyperfine tensors the isotropic part, $a=\frac{1}{3}\mathrm{Tr}(\overleftrightarrow{A})$, is given as a positive value. Subsequently the tensors that could be fitted are ordered with decreasing a values. The experimental results are given in Tables III and IV as obtained by fitting the O-*Mbc*1 and O-*Mbc*2 tensors; all the other oxygen tensors which could actually be observed in the experiment—O-*Mbc*3–O-*Mbc*8—were very similar and therefore not subjected to detailed fitting. Table III contains the data for both the hyperfine and the quadrupole tensors. The tensors are given as obtained for the orientation *ad*. Also the principal values and principal directions are calculated. In Table IV the reduced parameters a, b, and c are given. These were derived from the principal hyperfine values by equating them to $a+2b$, $a-b+c$, $a-b-c$. The a parameter represents the isotropic part of the hyperfine interaction, b determines the symmetric axial traceless tensor with principal values $+2b, -b, -b$, and c is the deviation from the axial symmetry. The parameters b and c are chosen such that $\mid b\mid > \mid c\mid$ which implies that sometimes $b<0$. As discussed in several textbooks and related publications it is possible to give an interpretation of these reduced parameters by linear combination of atomic orbitals (LCAO) analysis. However, if the signs of the parameters a and b are not the same the LCAO analysis is not applicable.

For deep centers with missing or dangling bonds the

TABLE II. The Zeeman frequency for a magnetic field of 1 T, the nuclear spin, the quadrupole moment, and the impurity concentrations as determined from ir absorption (Ref. 25), for the oxygen isotopes involved in the ENDOR experiment.

Isotope	I	Zeeman frequency (MHz)	Q (10^{-24} cm^2)	Concentration (cm^{-3})
^{16}O	0		0	2.2×10^{17}
^{17}O	$\frac{5}{2}$	5.772	-2.6×10^{-2}	1.2×10^{17}
^{18}O	0		0	0.6×10^{17}

TABLE III. Hyperfine and quadrupole parameters for the two fitted oxygen tensors. The tensors are given in the standard orientation *ad*, the tensor values, and the principal values are in kHz. Each principal value is followed by a normalized principal direction. The remaining six oxygen tensors (out of eight which could actually be observed in the experiment) were very similar to those fitted.

Shell	$\overleftrightarrow{A}$			i	A_i	$\mathbf{n}_i$
O-*Mbc*1	257.1	−0.9	0.9	1	258.5	(0.686, −0.515, 0.515)
	−0.9	252.9	−4.4	2	255.9	(0.728, 0.485, −0.485)
	0.9	−4.4	252.9	3	248.5	(0.000, 0.707, 0.707)
	66.4	−80.3	80.3	1	211.2	(0.617, −0.556, −0.556)
	−80.3	−33.2	−155.3	2	−22.7	(0.787, 0.436, −0.436)
	80.3	−155.3	−33.2	3	−188.5	(0.000, 0.707, 0.707)
Shell	$\overleftrightarrow{A}$			i	A_i	$\mathbf{n}_i$
O-*Mbc*2	208.8	−0.2	0.2	1	210.3	(0.164, −0.698, 0.698)
	−0.2	206.2	−4.1	2	208.7	(0.987, 0.116, −0.116)
	0.2	−4.1	206.2	3	202.1	(0.000, 0.707, 0.707)
	64.9	−80.2	80.2	1	211.7	(0.612, −0.560, 0.560)
	−80.2	−32.5	−156.5	2	−22.8	(0.791, 0.432, −0.432)
	80.2	−156.5	−32.5	3	−189.0	(0.000, 0.707, 0.707)

LCAO treatment is successful. However, for the shallow donors like P, As, Sb it turns out to be less applicable. From the LCAO analysis the localization η^2 of the electron spin on the nucleus involved can be calculated. For the oxygen tensors in Table III the corresponding LCAO localization values are less than 0.01%. The crystallographic (011) plane appears as forbidden in regard to the spin distribution. However one has to be careful with the interpretation of the calculated localization. To illustrate this point, consider the LCAO analysis when applied to the shallow donor phosphorus and the deep center V^-. One finds for phosphorus a total localization on the ligands of 13.7%.[28] Localizations around 0.01% on individual silicon neighbors are not uncommon, while these silicon atoms are not lying in forbidden planes. However in case of the V^- center (total localization larger than 100%), one finds localizations on silicon neighbors in the symmetry forbidden plane as high as 0.22%.[26]

Figure 4 gives an illustration of the similarity of the oxygen shells. The simulated ENDOR traces for the O-*Mbc*1 and O-*Mbc*2 shells are depicted as obtained for the EPR orientation *bc*. In the experiment the ENDOR traces were much more difficult to resolve due to the overlap of different EPR orientations giving rise to additional resonances. Since in our experiment the Si-NL10 spectrum was already in a late transformation stage its anisotropy was small and therefore different EPR orientations were hard to separate even in the *K*-band spectrometer that was used.

C. ^{27}Al ENDOR

The preliminary ENDOR experiment[24] also revealed the presence of aluminum in the Si-NL10 center. As a natural consequence an ^{27}Al ENDOR study was performed on the same sample.

The aluminum was present in the sample because the starting material was *p*-type aluminum doped. The aluminum has only one isotope with a nuclear spin $I=\frac{5}{2}$ and a quadrupole moment of 0.149 b. The Zeeman frequency for the ^{27}Al nucleus was in our experiment ~9.2 MHz.

Most of the Al ENDOR resonances occur for frequencies >6 MHz and are well separated from the oxygen ENDOR. Another empirical way to distinguish Al ENDOR from oxygen ENDOR is the linewidth which in the case of aluminum is ~10 kHz (FWHM). On the other hand also the presence of ENDOR from ^{29}Si could have been interfering; 4.7% of the Si atoms in the lattice surrounding the defect are of the ^{29}Si isotope with a nuclear spin of $I=\frac{1}{2}$. The corresponding Zeeman frequency is around 7.0 MHz, close to that for aluminum. However in our ENDOR study the ^{29}Si lines were found to be weak and broad and could easily be separated.

TABLE IV. Reduced tensor parameters of the oxygen hyperfine interactions in kHz, also the localization η^2 is given (see comment in text).

Shell	a	b	c	$\frac{a}{b}$	$\frac{b}{c}$	η^2 (%)
O-*Mbc*1	254.3	−2.9	−1.3	−88.3	2.2	<0.01
O-*Mbc*2	207.0	−2.5	−0.8	−83.9	3.2	<0.01

From the ENDOR experiment four Al tensors could be fitted, while there were indications for more tensors. They are summarized in Tables V and VI. Other tensors which could be observed with weaker intensities, labeled Al-*Mbc*4 and Al-*Mbc*5, were very similar to Al-*Mbc*3. The $g_N\mu_N/h$ value was also fitted here and found to be 11.098 MHz T^{-1}, which deviates slightly from the value of 11.094 MHz T^{-1} reported in the literature.[27] From the four tensors one was of class *T* (2*mm* symmetry), and three of the *Mbc* class. One of the *Mbc* tensors had almost 2*mm* symmetry as can be seen by inspecting Table V. The ENDOR spectrum of the aluminum tensors Al-*T*1 and Al-*Mbc*3 for EPR orientation *bc* is shown in Fig. 5. Again here, as in the case of oxygen, all the mirror class tensors found are of the same *Mbc* type indicating a planar structure of the Si-NL 10 center in one of the mirror planes.

D. Field-stepped ENDOR

The third experiment performed within the framework of this project was the field-stepped ENDOR (FSt ENDOR). This technique relates directly the ENDOR transition with the EPR line of its origin. As a result the high resolving power of ENDOR is used to unravel the structure of the EPR spectrum. For both oxygen and aluminum ENDOR the spin systems are characterized by $S=\frac{1}{2}$ and $I=\frac{5}{2}$. The corresponding level scheme is shown in Fig. 6, where the allowed EPR and ENDOR transitions are indicated. As can be seen ENDOR transitions 3↔4 and 9↔10 can be observed only on EPR transitions 3↔9 and 4↔10. In the present ENDOR experiment this means that both transitions attain their maximum intensity in the middle position between these two EPR transitions. The EPR transitions 3↔9 and 4↔10 are centered in the middle of the EPR line, which is not only inhomogeneously broadened by unresolved hyperfine interactions, but also by the superposition of the EPR from several species. So the ENDOR transitions 3↔4 and 9↔10 should reach their maximum intensity exactly at the center of the hyperfine broadened EPR line. For the different ENDOR shells we have tried to determine that position. However, due to experimental

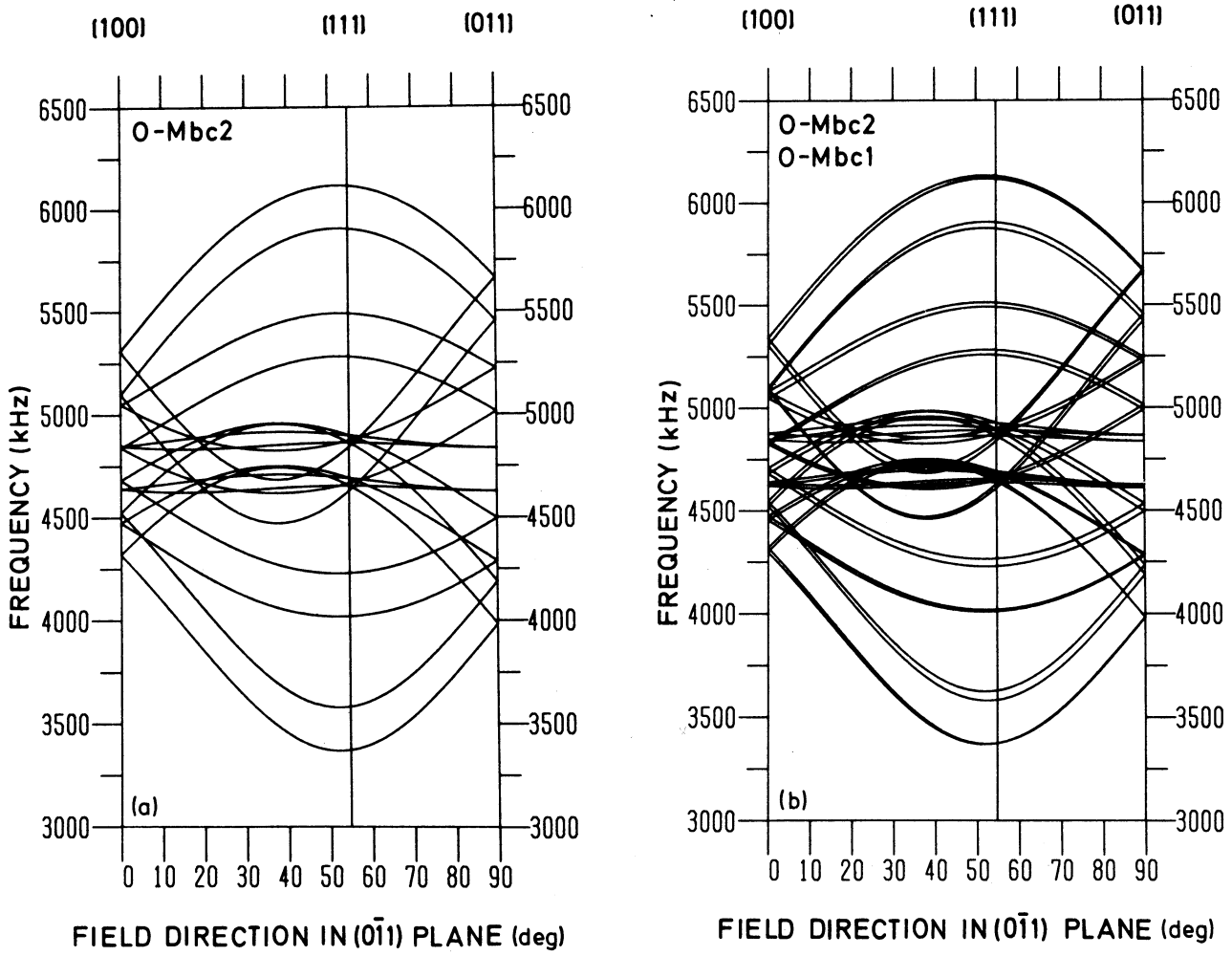

FIG. 4. Computer simulation of the angular ENDOR pattern corresponding to *bc* EPR orientation for (a) O-*Mbc*2 and (b) O-*Mbc*1 and O-*Mbc*2 tensors together.

TABLE V. Hyperfine and quadrupole parameters for the fitted aluminum tensors. The tensors are given in the standard orientation *ad*, the tensor values and the principal values are in kHz. Each principal value is followed by a normalized principal direction.

Shell		$\overleftrightarrow{A}$		i	A_i	$\mathbf{n}_i$
Al-*T*1	1062.5	0.0	0.0	1	1062.5	(1.000, 0.000, 0.000)
	0.0	926.5	−7.7	2	934.2	(0.000, −0.707, 0.707)
	0.0	−7.7	926.5	3	918.8	(0.000, 0.707, 0.707)
		$\overleftrightarrow{Q}$				
	26.6	0.0	0.0	1	950.8	(0.000, −0.707, 0.707)
	0.0	−13.3	−964.0	2	26.6	(1.000, 0.000, 0.000)
	0.0	−964.0	−13.3	3	−977.3	(0.000, 0.707, 0.707)
Shell		$\overleftrightarrow{A}$		i	A_i	$\mathbf{n}_i$
Al-*Mbc*1	1539.6	−61.7	61.7	1	1579.1	(0.911, −0.291, 0.291)
	−61.7	1355.6	−30.4	2	1346.6	(0.412, 0.644, −0.644)
	61.7	−30.4	1355.6	3	1325.2	(0.000, 0.707, 0.707)
		$\overleftrightarrow{Q}$				
	32.6	203.4	−203.4	1	1122.7	(0.255, 0.684, −0.684)
	203.4	−16.3	−1063.1	2	−43.3	(0.967, −0.180, 0.180)
	−203.4	−1063.1	−16.3	3	−1079.4	(0.000, 0.707, 0.707)
Shell		$\overleftrightarrow{A}$		i	A_i	$\mathbf{n}_i$
Al-*Mbc*2	1419.4	−19.4	19.4	1	1424.1	(0.986, −0.118, 0.118)
	−19.4	1250.7	−11.9	2	1257.9	(0.167, 0.697, −0.697)
	19.4	−11.9	1250.7	3	1238.9	(0.000, 0.707, 0.707)
		$\overleftrightarrow{Q}$				
	26.8	200.4	−200.4	1	1131.2	(0.249, 0.685, −0.685)
	200.4	−13.4	−1071.9	2	−45.9	(0.969, −0.176, 0.176)
	−200.4	−1071.9	−13.4	3	−1085.3	(0.000, 0.707, 0.707)
Shell		$\overleftrightarrow{A}$		i	A_i	$\mathbf{n}_i$
Al-*Mbc*3	1057.3	0.3	−0.3	1	1057.3	(1.000, 0.002, −0.002)
	0.3	917.8	−6.0	2	923.8	(0.003, −0.707, 0.707)
	−0.3	−6.0	917.8	3	911.8	(0.000, 0.707, 0.707)
		$\overleftrightarrow{Q}$				
	53.1	35.4	−35.4	1	824.1	(0.065, 0.706, −0.706)
	35.4	−26.5	−847.4	2	49.8	(0.998, −0.046, 0.046)
	−35.4	−847.4	−26.5	3	−873.9	(0.000, 0.707, 0.707)

reasons the accurate determination was possible only for the most intense ENDOR shells; for the weaker shells only a rough indication could be given.

The field-stepped ENDOR effect is illustrated for ^{17}O tensors in Fig. 7 and the results are summarized in Table VII.

1. Species and g shifting

The immediate conclusion from Table VII is that the Si-NL10 spectrum is indeed a superposition of a few different components. Moreover, the mutual separation of the components excludes their explanation by hyperfine interaction. So the EPR spectrum is inhomogeneously broadened not only by hyperfine structure but also by the presence of different species. In the EPR resonance linewidth of 0.4–0.5 mT neither the hyperfine interactions nor the species are resolved. Such resolution is possible only in the field-stepped ENDOR technique.

As mentioned earlier the Si-NL10 spectrum changes its g values on prolonged heat treatment at 400°–500 °C in

TABLE VI. Reduced tensor parameters of the aluminum hyperfine interactions in kHz, also the percentages of s and p character, α^2 and β^2, respectively, and the localization η^2 are given.

Shell	a	b	c	$\frac{a}{b}$	$\frac{b}{c}$	α^2 (%)	β^2 (%)	η^2 (%)
Al-*T*1	971.8	45.3	7.7	21.4	5.9	31	69	0.08
Al-*Mbc*1	1417.0	81.1	10.7	17.5	7.6	27	73	0.13
Al-*Mbc*2	1306.9	58.6	9.5	22.3	6.2	32	68	0.10
Al-*Mbc*3	964.3	46.5	6.0	20.7	7.7	31	69	0.08

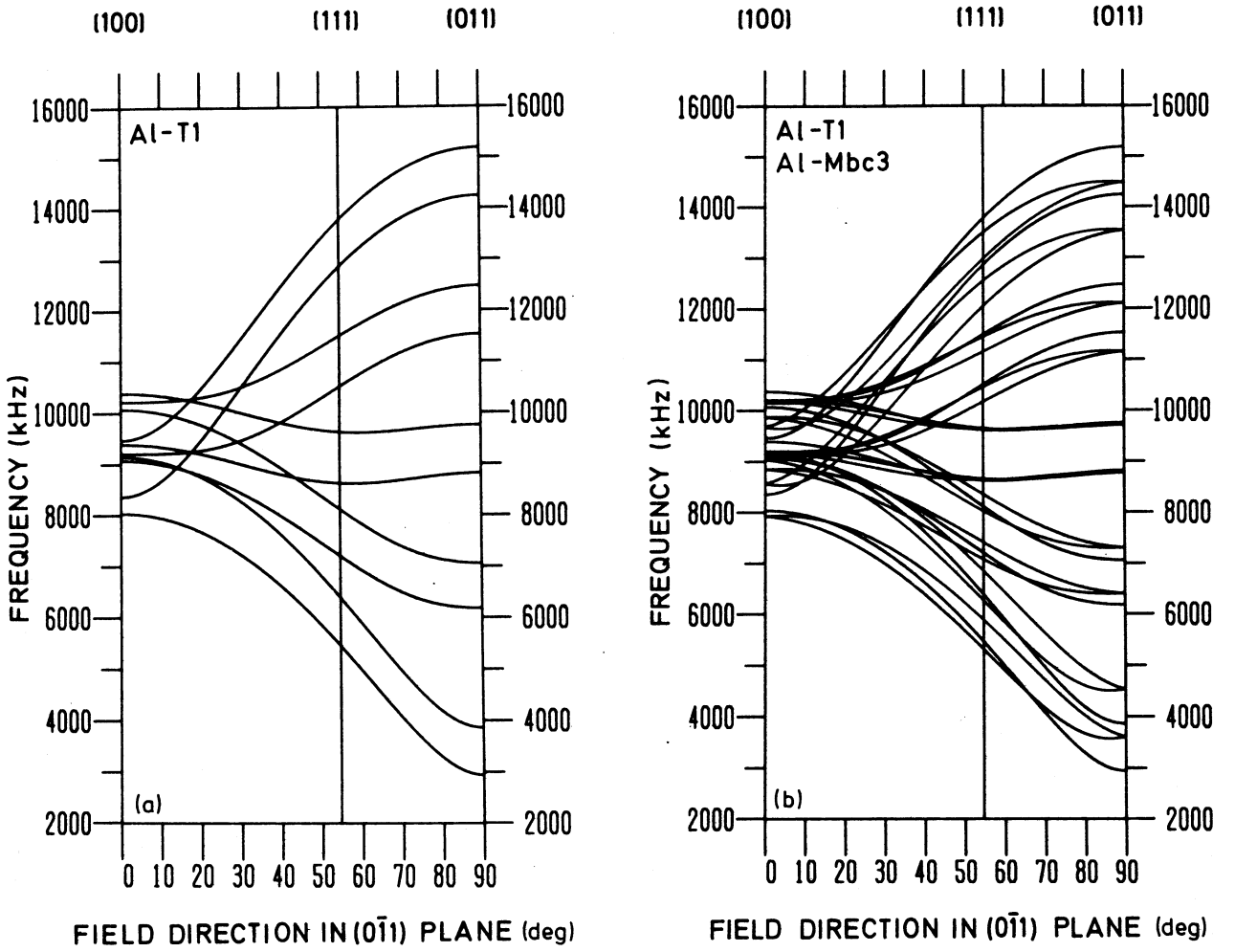

FIG. 5. Computer simulation of the angular ENDOR pattern corresponding to *bc* EPR orientation for (a) Al-$T1$ and (b) Al-$T1$ and Al-*Mbc*3 tensors together.

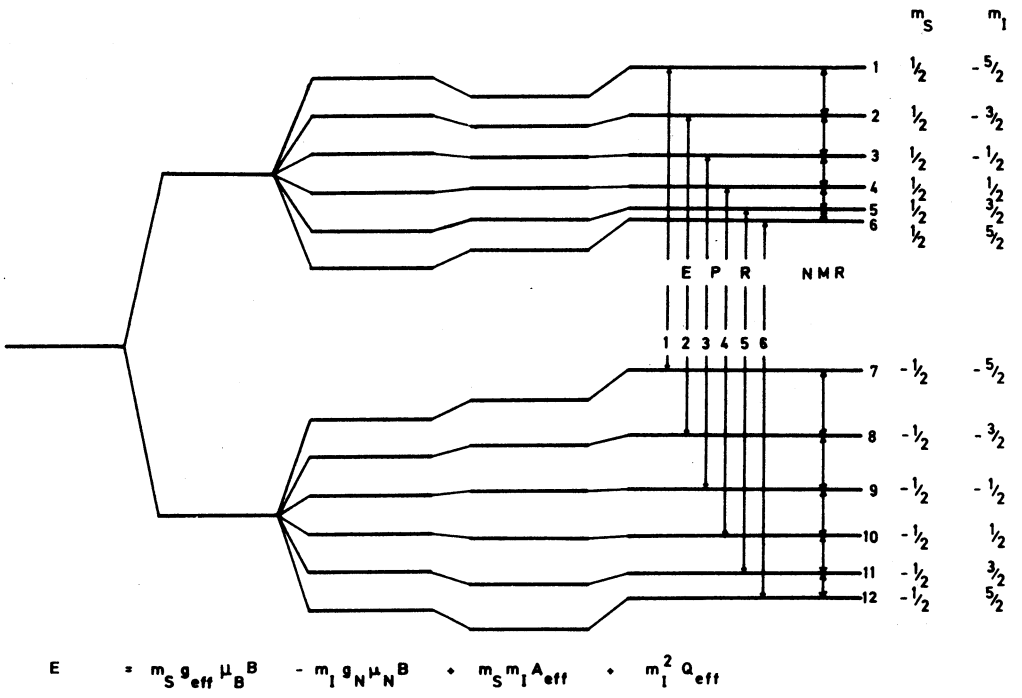

FIG. 6. Schematic representation of the energy-level scheme for the $S=\frac{1}{2}$, $I=\frac{5}{2}$ system. This scheme is applicable to both ^{17}O and ^{27}Al nuclei in the Si-NL10 center.

much the same way as Si-NL8. If one estimates the g values for the different species as revealed by FSt ENDOR, then the whole g shift can be accounted for. A varying concentration of different species results in a different average g value. A similar effect is probably responsible for the Si-NL8 g shifting.

2. *Correlation of oxygen and aluminum shells*

The field-stepped ENDOR technique can also help in correlating the oxygen with the aluminum shells since the oxygen and aluminum nuclei in one species have the same EPR resonance. The unambiguous correlation was possible only for the most prominent species. In particular one oxygen shell, O-*Mbc*2, and one aluminum, Al-*T*1, had their EPR line $+0.02-+0.03$ mT from the center of the total EPR resonance and so could mutually be correlated as coming from the same species. All other oxygen and aluminum shells have their EPR farther away from the center of the resonance line and therefore belong to species of lower concentrations.

The Al-*Mbc*1 and Al-*Mbc*2 tensors seem to correspond to earlier and the Al-*Mbc*3 to later annealing stages. The ENDOR measurements for aluminum-doped heat-treated Czochralski-grown silicon showed that in those samples the same Al-*T*1 and Al-*Mbc*3 shells could be observed. The Al-*Mbc*1 and Al-*Mbc*2 shells were not seen even in a sample which was heat treated for only 15 h. It appears then that those tensors correspond to early species which are formed only in material with low oxygen concentration. The Al-*Mbc*4 and Al-*Mbc*5 shells which were only weak in our FZ sample became dominating for longer annealed Czochralski-grown silicon samples. Also new shells appeared, which were all *Mbc* class and similar to the Al *Mbc*3–*Mbc*5 shells.

3. *The symmetry of the Si-NL10 center*

From the EPR measurements the symmetry of the Si-NL10 spectrum was found to be $2mm$. The FSt ENDOR technique with its high resolution can verify this now separately for every component of the EPR resonance. This issue is of crucial importance in the modeling of the Si-NL10 center as directly related to the question of how many aluminum (and oxygen) nuclei are incorporated in the earlier and later species of the center. According to Table I they must have at least two aluminum nuclei, because all the remaining shells are of the M class. However Table I is valid only under the assumption of $2mm$

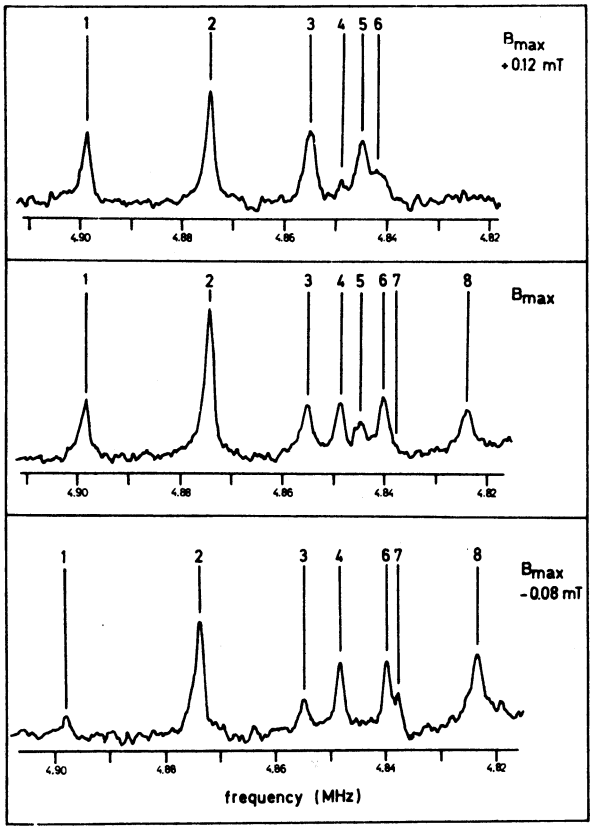

FIG. 7. The illustration of the field-stepped ENDOR effect for the oxygen tensors. Numbers 1–8 correspond to oxygen tensors O-*Mbc*1–O-*Mbc*8, respectively. The magnetic field is in the [011] direction and B_{max} corresponds to the magnetic field position in the center of the EPR line.

TABLE VII. EPR line positions for the oxygen and aluminum shells derived from field-stepped ENDOR. Positions are given with respect to the maximum of the EPR line for orientation *bc* and the magnetic field in the [011] direction. The sign is chosen to be positive for the earlier transformation stages of the Si-NL10 spectrum.

Oxygen		Aluminum	
Shell	Position (mT)	Shell	Position (mT)
O-*Mbc*1	$+0.06-+0.08$	Al-*T*1	$+0.02$
O-*Mbc*2	$+0.02$	Al-*Mbc*1	$\sim+0.13$
O-*Mbc*3	$+0.06-+0.08$	Al-*Mbc*2	$\sim+0.07$
O-*Mbc*4	$-0.02--0.04$	Al-*Mbc*3	~-0.04
O-*Mbc*5	$+0.07-+0.10$	Al-*Mbc*4	~-0.08
O-*Mbc*6	~-0.04	Al-*Mbc*5	<-0.08
O-*Mbc*7	<-0.08		
O-*Mbc*8	~-0.04		

TABLE VIII. Properties of the different types of hyperfine tensors and associated shells for a spectrum with mirror plane symmetry. N_{at} is the number of atoms per shell and N_{el} is the number of independent tensor elements. The number of ENDOR lines is indicated for the three high-symmetry directions in the $(0\bar{1}1)$ plane.

Class	Symmetry	N_{el}	N_{at}	Atom positions	No. of lines, B‖ [100]	[111]	[011]
M	*m*	4	1	on mirror plane	2	3	4
G	1	6	2	off mirror plane	3	4	6

symmetry of the EPR spectrum. If the symmetry is not 2*mm* but *m* then a different table has to be written (see Table VIII). As can be seen, only two tensor classes are possible and a mirror class tensor corresponds now to a shell of one nucleus only. Let us now consider how the field-stepped ENDOR can unravel the actual symmetry of the EPR. Consider the ENDOR angular dependence of a *Mbc* tensor produced for EPR orientation *bc*. If the EPR symmetry were 2*mm* then its two ENDOR lines should correspond to the same EPR line. The two lines would correspond to different EPR orientations if the EPR were of mirror plane symmetry. Based on this phenomenon the field-stepped ENDOR measurements unambiguously establish that the Al-*Mbc*1 and Al-*Mbc*3 tensors actually belong to an EPR resonance of the mirror class symmetry. Similar conclusion is most probably true also for the Al-*Mbc*2 tensor whose weak intensity obstructs the FSt ENDOR experiment. However the splitting due to the lower symmetry is very small and cannot be resolved in EPR ($\sim$0.03 mT). Figure 8 illustrates the effect as experimentally observed for the Al-*Mbc*3 shell. This leads to the conclusion that all the species have only one aluminum atom incorporated in their structure. For one of them the aluminum atom is on the 2*mm* axis while for all the others it is no longer on the twofold axis of the defect although it remains on the mirror plane, the same that incorporates the oxygen atoms. The symmetry is then lowered from 2*mm* to *m*. Because the localization of the paramagnetic electron on the aluminum is so low, it can hardly notice the presence of the aluminum; the EPR spectrum therefore remains almost 2*mm*.

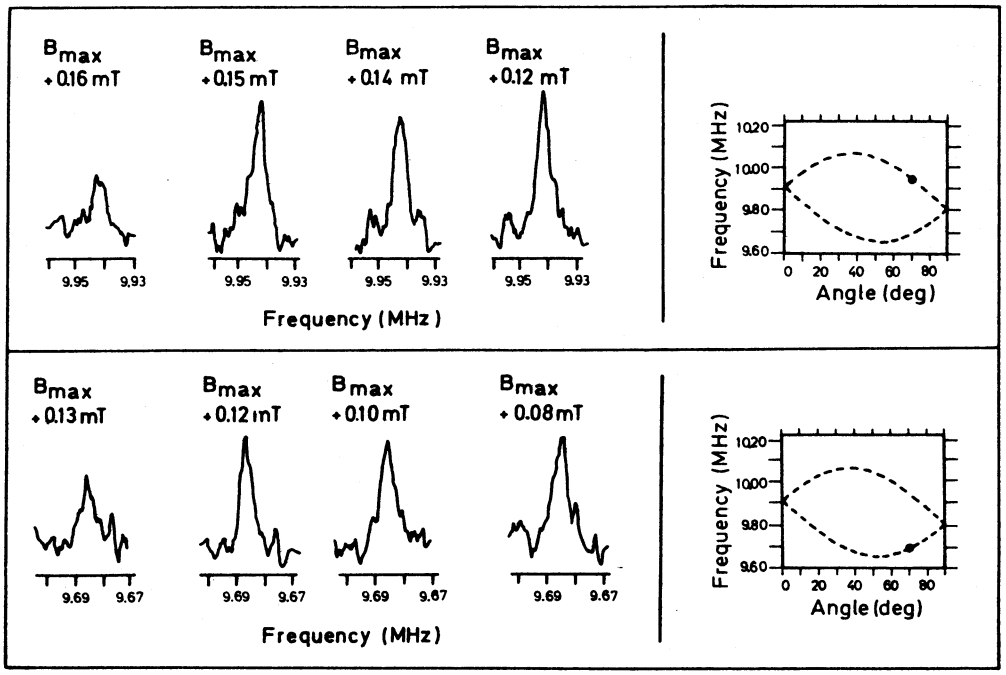

FIG. 8. The illustration of the field-stepped ENDOR technique as applied to reveal the symmetry of the EPR resonance. The ENDOR signal for the two resonances of one loop of the Al-*Mbc*3 tensor corresponding to the *bc* EPR orientation (as indicated on the right-hand side of the figure) was recorded as a function of the magnetic field, with respect to the center of the EPR resonance B_{max}. As shown the two resonances originate from different EPR.

V. DISCUSSION

A. Quadrupole interaction

The quadrupole interaction takes place between the nuclear quadrupole moment and the electric field gradient at the site of the nucleus and its components are given by

$$Q_{ij}=\frac{eQ}{2I(2I-1)}\frac{\partial^2 V}{\partial x_i \partial x_j} , \tag{7}$$

where e is the electronic charge, Q is the quadrupole moment, I is the nuclear spin, and V is the electrostatic potential. The quadrupole interaction tensor $\tilde{Q}$ is a measure of the total unbalanced charge density around the nucleus (and not only the spin density).

As a first contribution to an unbalanced charge density around the nucleus one can calculate the effect of a distant charge. A positive point charge e at a distance r yields an axially symmetric quadrupole tensor, with its axial direction parallel to the line connecting the point charge and the nucleus and with principal values $(2q,-q,-q)$. With Eq. (7) one can evaluate

$$q=\frac{1}{4\pi\epsilon_0}\frac{e^2Q}{2I(2I-1)}\frac{1}{r^3} . \tag{8}$$

In Table IX the quadrupole interaction is calculated for a single positive point charge at a nearest-neighbor distance ($r=0.235$ nm) from an oxygen or an aluminum nucleus. As can be seen by comparing the numbers in Table IX with the experimental quadrupole tensors the point-charge contribution is much too small to explain the experimental data.

A bigger contribution to the unbalanced charge density arises from an unbalanced charge at the nucleus itself. With use of Eq. (7) one can calculate the quadrupole interaction of a single electron in a p orbital. A single p electron gives also an axially symmetric quadrupole tensor with

$$q=-\frac{1}{4\pi\epsilon_0}\frac{e^2Q}{2I(2I-1)}\frac{2}{5}\langle r^{-3}\rangle_p . \tag{9}$$

TABLE IX. Quadrupole parameters q for a positive point charge at 0.235 nm from an oxygen or aluminum nucleus, compared with the contributions from an electron in a p orbital centered around the nuclei. The values are calculated in kHz with use of Eqs. (8) and (9). Q values are taken from Ref. 27.

nucleus	Q (10^{-24} cm^2)	point charge (kHz)	p orbital (kHz)
^{17}O	-2.6×10^{-2}	−3.5	707
^{27}Al	0.149	19.9	−1039

The values calculated for a free atom p orbital at an oxygen and an aluminum nucleus are also given in Table IX.[29]

In case of a nucleus with four occupied p orbitals in $\langle 111\rangle$ directions ($[\bar{1}11],[1\bar{1}1],[11\bar{1}],[\bar{1}\,\bar{1}\,\bar{1}]$) the four contributions to the quadrupole tensor cancel and no quadrupole interaction can be observed. The values calculated with Eq. (9) are big enough to account for the experimentally observed values. However, as can be seen from Tables III and V, the experimental quadrupole tensors are far from axial and as such, cannot result from a single contribution. Therefore for further analysis they have to be decomposed.

There is no unique solution to this problem. One particular possibility is to decompose the tensor into two axial components with equal principal values, but different orientations. Any experimental tensor, with principal values (Q_1,Q_2,Q_3), can be decomposed in this way:

$$Q_1=-2q , \tag{10a}$$

$$Q_2=q[1+3\cos(\alpha)] , \tag{10b}$$

$$Q_3=q[1-3\cos(\alpha)] . \tag{10c}$$

By applying Eq. (10) one gets the angle α between the two axial directions of the quadrupole tensors and the value of the axial component q. The principal values of the two equal axial tensors are then $(-q,-q,2q)$. Figure 9 shows how the axial directions of the two decomposed tensors are related to the principal directions of the experimental tensor. The principal directions labeled 1, 2, and 3 have their principal values Q_1, Q_2, and Q_3, respectively.

B. Position of the oxygen atom

In decomposing the oxygen quadrupole interactions it is reasonable to assume that the oxygen is bonded to two atoms. The oxygen atom has six valence electrons, and is eager to form two bonds to obtain the inert gas configuration. Let us first give an illustration of the method by using the ENDOR data of a known defect. The A center consists of a vacancy trapped by an oxygen atom. The oxygen atom that was first in its normal interstitial puckered bond position now passivates two dangling bonds by bonding with two of the first neighbors of the vacancy. The quadrupole tensor for the oxygen atom is presented in Table X.[30] The tensor is given in an orientation in which the oxygen has two bonds in the (011) plane. Following our decomposition scheme direction 1 will correspond here to the [011] direction and direction 2 to the [100] direction. Applying Eq. (10) we get: $q=-86.85$ kHz and $\alpha=155°$. According to calculations performed by Canuto and Fazzio[31] this angle should be $\alpha=164.8°$, which is very close to the result of the decomposition of the quadrupole tensor.

If the oxygen atom was free and not in a crystal we should expect a q value of 707 kHz. However, the crystal

is disturbing this ideal situation. For instance the bonds with the silicon atoms are partially ionic. The electronegativity difference between oxygen and silicon is 1.7.[32] According to Pauling[32] the ionicity of a single bond is

$$f_i = 1 - \exp\left[-\frac{(X_A - X_B)^2}{4}\right], \tag{11}$$

where $X_A - X_B$ is the difference in electronegativity between atoms A and B. For the Si—O bond Eq. (11) gives $f_i = 0.51$. This should be compared with a typical ionic bond of NaCl where $f_i = 0.67$. So as a result one can expect that some charge will be drawn towards the oxygen, thus reducing the field gradient at the oxygen nucleus.

Let us consider now the quadrupole tensors of the Si-NL10 center. Inspecting Table III, one can notice that the two quadrupole tensors are almost identical. For the standard orientation *ad* the oxygen atoms are lying in the (011) plane. We assume now that the oxygen is bonded and that there are no lone-pair p orbitals. The bonded atoms are lying in principal direction 3 of the decomposition scheme. The principal directions of the quadrupole tensor are close to [011], [21$\bar{1}$], and [1$\bar{1}$1]. It is then most natural to choose [1$\bar{1}$1] as the decomposition direction 3. The other directions then follow as the oxygen atoms have to be in the (011) plane. Principal direction 1 in the decomposition is then [011] and direction 2 is [21$\bar{1}$]. Applying Eq. (10) one gets: $\alpha = 114.4°, q = 94.3$ kHz. The value of 94 kHz seems to be reasonable when compared to 87 kHz obtained for the A center.

This interpretation of the principal directions and the angle α gives almost the usual interstitial puckered bond position for the oxygen atom. The bond angle for the isolated interstitial oxygen has been measured by Bosomworth *et al.*[33] They find a Si—O—Si bond angle of $\alpha = 162°$. This value of 162° has been calculated under the assumption that the Si—Si distance is the same as for an undistorted silicon crystal. Calculations of Snyder and Corbett[16] by *ab initio* molecular orbital calculations of interstitial oxygen in silicon show that the Si—O—Si bond angle is $\alpha = 149°$. The deviation with the bond angle we calculated is possibly caused by the fact that the interstitial oxygen is now incorporated in a defect, distortions of the surroundings of the Si—O—Si structure affect the bond angle. Although the decomposition is not unique, the result appears remarkably credible.

C. Position of the aluminum atom

Also the quadrupole tensors of the aluminum shells are all far from axial. They are similar to each other and, in a way, similar to the oxygen quadrupole tensors. We first consider the quadrupole tensor of the shell Al-$T1$ which consists of one Al nucleus on the twofold axis. Judging from the magnitude of the interaction also here the contribution from p orbitals has to be considered.

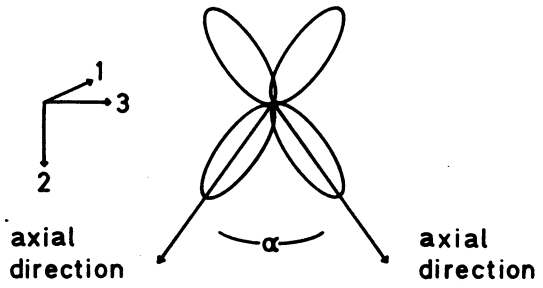

FIG. 9. Decomposition of an arbitrary traceless tensor into two equal axial components. The directions and parameter α as used in the text are indicated.

If aluminum has a single $3p$ orbital centered around its nucleus then the resulting quadrupole tensor is axial. The same holds if there are three p electrons in three of the four available ⟨111⟩ directions. So here again the decomposition into two axial tensors appears natural. We will further assume that both axial contributions are of equal magnitude. This is not unreasonable because the symmetry of the Al-$T1$ shell suggests that the defect has locally perfect $2mm$ symmetry. The principal directions of the experimental tensor are [0$\bar{1}$1], [100], and [011]. Therefore we should choose [100] as decomposition direction 2 (Fig. 9). However, nothing is known about other decomposition directions; for them two possibilities exist which are summarized in Table XI. The experiment cannot decide which one should be preferred.

The resulting angle α given in Table XI is almost equal to the normal angle between two ⟨111⟩ directions in the silicon lattice (109.45°). This result is again very plausible, supporting the decomposition into two equal axial tensors. The calculated value of q is equal to about half the contribution expected for a $3p$ orbital at an isolated aluminum nucleus. Since the electronegativity difference for silicon and aluminum is small, only 0.3, the correction for charge attraction in the bond will also be small. However the extent to which the quadrupole interaction is influenced by the rest of the lattice is not known. When considering the charge state of the aluminum atom two possible cases exist.

(1) If the influence from the lattice is negligible, then the quadrupole interaction can be caused by only one electron, which is spending half of its time in each of the

TABLE X. Quadrupole parameters for the oxygen tensor in the A-center after van Kemp (Ref. 30). The tensor values and the principal values are in kHz. Each principal value is followed by a normalized principal direction.

Shell	$\vec{\vec{Q}}$			i	Q_i	$\mathbf{n}_i$
	149.3	0	0	1	173.7	(0.000, 0.707, 0.707)
^{17}O	0	−74.6	248.3	2	149.3	(1.000, 0.000, 0.000)
	0	248.3	−74.6	3	−323.0	(0.000, −0.707, 0.707)

TABLE XI. Decomposition parameters for the quadrupole tensor of the Al-$T1$ shell.

Case	Decomposition direction 1	2	3	q (kHz)	α (deg)
I	[011]	[100]	[0$\bar{1}$1]	488.7	108.4
II	[0$\bar{1}$1]	[100]	[011]	−475.4	110.6

two p orbitals. From quadrupole data, it is not possible to say whether the interaction is caused by the presence or the lack of an electron. The quadrupole interaction for an aluminum nucleus with four ⟨111⟩-directed sp^3 orbitals two of which are half occupied, is the same as for an aluminum nucleus with two half occupied sp^3 orbitals. The difference between those two situations is only in sign, which, however, cannot be determined in our experiment. In such case Al^0 and Al^{2+} charge states are possible.

(2) If we now assume that the lattice influence on the quadrupole interaction is considerable, and that the quadrupole interaction is caused by the presence or the absence of two complete sp^3 orbitals, then the possible charge state would be Al^+.

Therefore, as far as the quadrupole interaction is concerned all three charge states Al^0, Al^+, and Al^{2+} are possible. Out of these three only the Al^+ charge state is nonparamagnetic and the fact that no large aluminum hyperfine interaction is observed slightly points towards that case.

Another important question which cannot be answered in our experiment is whether the aluminum is bonded to the silicon lattice in a substitutional position or is interstitial and remains nonbonded. In the latter case the quadrupole interaction would arise from the lone-pair 3p orbitals directed in space along ⟨111⟩ directions by the crystal field.

For the other Al shells the quadrupole tensors could be decomposed in the same way. Table XII summarizes the results. The principal directions of these tensors are close to [100], [0$\bar{1}$1], and [011]. The angle α and quadrupole parameter q are close to the values calculated for the Al-$T1$ shell. A similar interpretation can then be proposed. For the *Mbc* shells, whose symmetry is no longer 2*mm*, the aluminum nucleus is not anymore on the twofold axis. This means, that upon prolonged heat treatment, either the aluminum is moving (which is rather improbable unless interstitial diffusion takes place) or the center is growing.

VI. THE MICROSCOPIC MODEL OF THE Si-NL10 CENTER

A. Basic model

We can now propose a detailed structural model for the center responsible for the Si-NL10 EPR spectrum. We have already shown that indeed a variety of similar species is produced depending on duration of the annealing time (and most probably the annealing temperature as it will influence the diffusion speed). We have also shown, by means of field-stepped ENDOR, the correlation between the two most intense ENDOR tensors—Al-$T1$ for aluminum and O-*Mbc*2 for oxygen. Moreover it is clear from our experiment that those two tensors are the only ones which can be mutually correlated and they correspond to the strongest component of the EPR spectrum. Therefore we can conclude that although there are several different Si-NL10 species present in our sample the one which is present in the highest concentration is described by one oxygen and one aluminum ENDOR tensor. From now on we will refer to that center as Si:Al-NL10-1. Following the earlier discussion about the possible positions of aluminum and oxygen atoms the structural model can be proposed as depicted in Fig. 10. Since our experiment cannot distinguish between substitutional and tetrahedral interstitial positions for the aluminum atom another similar model could be constructed with the aluminum on the substitutional site. However, if the aluminum atom would stay at its substitutional position then the whole defect would most probably have a shallow acceptor character while the resistivity measurements indicate that the material is becoming intrinsic with increased annealing time (the effect being independent of the initial acceptor concentration). The absence of the (relatively shallow) acceptors can also be deduced from the fact that the Si-NL8 spectrum can no longer be observed by EPR. If the acceptor centers were actually present at least some of the NL8 TD's would ionize to the paramagnetic NL8 $(TD)^+$ state giving rise

TABLE XII. Decomposition parameters of the quadrupole tensor of the three fitted Al-*Mbc* shells. The decomposition direction is expressed as the deviation δ from the indicated closest crystal axis.

Shell	Case	Decomposition direction 1 axis	1 δ	2 axis	2 δ	3 axis	3 δ	q (kHz)	α (deg)
Mbc-1	*I*	[011]	0	[100]	14.8	[01$\bar{1}$]	14.8	539.7	111.1
	II	[01$\bar{1}$]	14.8	[100]	14.8	[011]	0	−561.4	107.9
Mbc-2	*I*	[011]	0	[100]	14.3	[01$\bar{1}$]	14.3	542.7	111.2
	II	[01$\bar{1}$]	14.3	[100]	14.3	[011]	0	−565.6	107.8
Mbc-3	*I*	[011]	0	[100]	3.6	[01$\bar{1}$]	3.6	437.0	107.2
	II	[01$\bar{1}$]	3.6	[100]	3.6	[011]	0	−412.1	111.9

to the Si-NL8 spectrum.

In view of the above the model depicted in Fig. 10, with the aluminum on a tetrahedral interstitial position, seems to be the more likely candidate, although it involves a vacancy which by itself is a deep defect. However, the presence of oxygen atoms could strongly influence the position of energy levels in the forbidden gap. A situation which is to a certain extent similar takes place in the case of the Si A center as compared to the isolated vacancy; here the presence of an oxygen atom passivating two broken bonds gives also rise to a relatively shallow energy level. The assumption that indeed the vacancy constitutes part of the Si:Al-NL10-1 is further justified by the compressive stress which must arise as a result of the oxygen aggregation taking place not just in one plane but also along one direction; the vacancy would provide a natural way to accommodate that stress.

B. Transformation of the Si-NL10 centers

Although the Si:Al-NL10-1 center is the dominant one in our sample it is not the only center present. As revealed by the FSt ENDOR studies the next species in terms of the annealing time development is characterized again by only one aluminum ENDOR tensor, namely, Al-*Mbc*3. Our studies on Czochralski-grown aluminum-doped silicon showed that species to be dominant for the samples with relatively short annealing time of a few hours. We will refer to this center as Si:Al-NL10-2. Our results indicate that it incorporates also only one aluminum atom but no longer on the twofold axis as the overall symmetry of the center is now lowered to m. The precise number of the oxygen ENDOR tensors corresponding to Si:Al-NL10-2, although more difficult to determine, is most likely 3 (as may be deduced from Table VII and Fig. 7): O-*Mbc*4, O-*Mbc*6, and O-*Mbc*8.

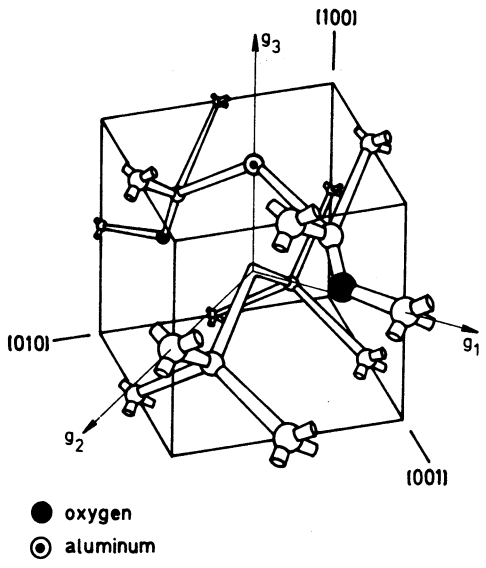

FIG. 10. Structural model for the Si:Al-NL10-1 center. The aluminum atom is shown on a tetrahedral interstitial position; however the normal substitutional site cannot be excluded. Defect orientation *ad*.

All those tensors belong to the *Mbc* symmetry class and are very similar. Since the symmetry of the Si:Al-NL10-2 center is m then the most probable model for that center should incorporate one aluminum and three oxygen atoms. Moreover, since the tensors are very similar to those characteristic for the Si:Al-NL10-1 center, the atomic configuration of those two centers should also be similar. Therefore we propose that the NL10-1 center transforms into NL10-2 by capturing one more oxygen; the third oxygen atom takes one of the two nearest bond-centered positions available along the $[0\bar{1}1]$ crystallographic direction.

Since Si:Al-NL10-1 and Si:Al-NL10-2 are the dominant species present in our sample relatively less can be said about further transformation of the center. Fortunately some information could be obtained here from our studies on aluminum-doped Czochralski-grown silicon. The results show that the next species has again only one aluminum tensor Al-*Mbc*4, again very similar to Al-T1 and Al-*Mbc*3. Those results are confirmed in the FSt ENDOR experiment, which indicates an EPR position related with the Al-*Mbc*4 tensor at about 80–90 μT from the maximum of the EPR signal for our sample. This also indicates that here only one aluminum atom is involved and that its position is the same as in earlier transformation stages. Unfortunately the studies on Czochralski-grown silicon could not bring any information on the oxygen incorporation in the later species due to very low natural abundance of the magnetic ^{17}O isotope. We propose that the transformation of Si:Al-NL10 centers continues as in the first stage, by further growth of the oxygen chain along $[0\bar{1}1]$.

As can be found in Table V, ENDOR studies revealed two more aluminum tensors that have not been discussed yet: Al-*Mbc*1 and Al-*Mbc*2. Now we will address that issue. The relevant experimental information can be summarized as follows.

(1) The Al-*Mbc*1 and Al-*Mbc*2 tensors are similar and significantly different from Al-T1 and Al-*Mbc*3 and/or Al-*Mbc*4. The difference is mainly in the hyperfine component, while the quadrupole interaction remains almost unchanged.

(2) FSt ENDOR studies show that the maximum for Al-*Mbc*1 and *Mbc*2 tensors can be found at approximately 140–120 and 90–70 μT, respectively. This observation can be taken as an indication that those tensors correspond to earlier transformation stages of the Si:Al-NL10 center. However, as can be seen in Fig. 1, this would lead to ΔB values which can never be observed between the maxima of the EPR lines for aluminum-doped silicon, but can only be found for boron-doped material. Moreover, it is difficult to imagine a center of the earlier transformation stage than Si:Al-NL10-1 but similar to it (and we would need two such centers).

(3) The shift for the position of the maximum between Al-*Mbc*1 ($+130$ μT) and Al-*Mbc*2 ($+70$ μT) is similar to that between Al-T1 ($+20$ μT) and Al-*Mbc*3 (-40 μT), just as the transformation lines for various acceptor dopings on Fig. 1 are parallel.

(4) Although the number of oxygen tensors corresponding to Al-*Mbc*1 and Al-*Mbc*2 is difficult to establish

it seems most likely that it is 3 for Al-*Mbc*1 (in close analogy to Al-*Mbc*3).

(5) The Al-*Mbc*1 and Al-*Mbc*2 tensors are not observed in Czochralski-grown silicon doped with aluminum, not even for very short annealing times.

On the basis of the above experimental findings we propose that the Al-*Mbc*1 and Al-*Mbc*2 tensors correspond to defects similar to those responsible for Al-*T*1 and Al-*Mbc*3 but where the central vacancy has been created by removal of a silicon and not an aluminum atom. Under the assumption that the oxygen's affinity to aluminum will cause its aggregation in the vicinity of the aluminum atoms, and assuming further that creation of a single vacancy is sufficient to release the compressive stress generated by such oxygen aggregation, it is indeed possible in early stages of the Si:Al-NL10 center creation that the silicon and not the aluminum atom is "flipped" into the interstitial position when simultaneously surrounded by two oxygens. The silicon self-interstitial created in that way will then react with a nearby substitutional aluminum atom by Watkins replacement mechanism[34] producing eventually interstitial aluminum which will then diffuse (interstitially) to its favorite position along the [100] direction against the vacancy—as in the Si:Al-NL10-1 center. The Al-*Mbc*1 and Al-*Mbc*2 tensors would then correspond to the aluminum atom positioned on the interstitial sites adjacent to the one responsible for Al-*T*1. The centers giving rise to the Al-*Mbc*1 and Al-*Mbc*2 tensors are then possible only in the early stage of the agglomeration and/or transformation process, the situation being automatically corrected as soon as the aluminum interstitial moves on the axis of the defect. In that way one can understand that the Al-*Mbc*1 and Al-*Mbc*2 tensors can be observed in our FZ oxygen-diffused sample and not in Czochralski-grown material for which the oxygen concentration is 2–3 times higher and the transformation kinetics, respectively, faster.

C. Identification of the Si-NL10 center

Let us summarize the features of the Si:Al-NL10 center model as developed so far on the basis of our present detailed study. First, it is a center which can be created in oxygenrich silicon by annealing in the temperature region for thermal donor formation at ~450 °C. Its creation is independent of the doping, be it *p* type or *n* type. Also the loss of Si-NL10 centers at higher temperatures (550 °C) coincides with removal of the thermal donors as measured by resistivity.[5] Secondly, the center develops several species with annealing time, growing by subsequent addition of bond-centered interstitial oxygen atoms along the [0$\bar{1}$1] crystallographic direction. The most probable model of the smallest species involves a vacancy and two oxygen atoms. Thirdly, in the case of aluminum-doped silicon, oxygen-aluminum affinity will force aggregation in the vicinity of aluminum atoms; in that case the majority of Si-NL10 centers will incorporate *one* aluminum atom, preferably in the interstitial position. At the same time resistivity measurements indicate that the center exhibits donor character at room temperature. All those features are characteristic of silicon thermal donors.

On this basis two interpretations seem to be plausible. According to one of them, the Si-NL10 center is an acceptor based oxygen complex, growing in oxygenrich silicon in parallel to NL8 TD's. It should be very similar to NL8 TD's, the presence of the acceptor possibly changing it into a shallow single donor with effective-mass character. There are, however, several arguments against such an interpretation; the most important one is the concentration argument, as the Si-NL10 centers seem to be formed at a concentration exceeding that of available acceptors[5] and—in *n*-type, phosphorus-doped silicon—in concentration much higher than the probable level of counterdoping.[22,35]

Another possibility is to interpret the Si-NL10 spectrum as arising from the acceptor state of the NL8 TD, namely, NL8 $(TD)^-$. Indeed, if an oxygen-surrounded vacancy constitutes the core of the Si-NL10 center as suggested by the interpretation of our ENDOR data, then it follows naturally that, in analogy with a vacancy center in silicon, not only neutral and donor but also acceptorlike states may be expected. It should again be stressed here, that the analogy to the isolated vacancy in silicon is very limited, as the presence of the growing oxygen cluster severely alters its properties. Although the acceptor character of the Si-NL10 center would have to be investigated in detail[35] already the existing data are indicative. Here the strong dependence of the Si-NL10 spectrum intensity on illumination in *p*-type material has to be compared with a complete lack of such effect for *n* type.[22,35] This is very difficult to reconcile with a single shallow donor character, especially if one bears in mind that the intensity increase takes place regardless of whether the acceptors are being removed (as in the case of aluminum doping) or not (as for boron) by the creation of Si-NL10 centers. On the other hand, for boron-doped samples, where boron atoms do not take part in oxygen aggregation, retaining their acceptor character, the Si-NL8 [NL8 $(TD)^+$] spectrum is the most intense while Si-NL10 is relatively weak. The position of the energy level associated with Si-NL10 also requires further studies, but in our view it should be a very deep acceptor level with its energy close to that of the phosphorus donor.[35]

If the identification of the Si-NL10 center with NL8 $(TD)^-$ is confirmed, then the core of the NL8 TD will be vacancylike, with the remarkable phenomenon of a deep center that becomes shallow by the presence of oxygen atoms in its direct neighborhood.

VII. SUMMARY AND CONCLUSIONS

Three independent ENDOR experiments have been performed on the Si-NL10 center in the same sample of FZ aluminum-doped silicon diffused with ^{17}O isotopically enriched oxygen.

The oxygen ENDOR study revealed that the Si-NL10 center is an oxygen aggregate. During 450 °C annealing several different species develop by subsequent addition of oxygen atoms along the ⟨011⟩ crystallographic direction in the (011) plane. The experimental data show that the oxygen atoms in the center occupy their "normal"

puckered bond-centered interstitial position with a bond angle of $\sim 114°$.

The ^{27}Al ENDOR study has shown that a single aluminum atom was present in the center regardless of its growth stage. The position of the aluminum was argued to be rather tetrahedral interstitial than substitutional, but the experiment cannot provide a decisive answer here. The conclusion of the aluminum involvement in the Si-NL10 center was unexpected and difficult to reconcile with the fact that the Si-NL10 spectrum is not characteristic for aluminum-doped silicon and can be observed in any heat-treated oxygenrich silicon regardless of its doping. It has been proposed that aluminum is not really necessary for the formation of the Si-NL10 center. Due to its affinity to oxygen it takes, when present, an active part in the oxygen aggregation. In that case the aluminum atom provides a very convenient means of probing into the aggregation mechanism. Additional valuable information was obtained from a FSt ENDOR experiment. The most important results are the following.

(1) Different Si-NL10 species have slightly different EPR spectra thus providing a natural explanation for the so-called "g-shifting effect."

(2) The basic Si:Al-NL10 species consists of a single aluminum and two oxygen atoms. The center has $2mm$ symmetry with the aluminum atom located on the twofold axis of the defect.

(3) The second species to develop has no longer exactly $2mm$-type symmetry, although the deviation towards the lower m-type symmetry is very small and as such not resolved in the EPR experiment. The defect incorporates again only one aluminum atom and (most probably) three oxygen atoms. The later species also incorporate a single aluminum atom and a subsequently growing number of oxygens.

(4) In the case of relatively low oxygen contents centers similar to the two discussed above but (most probably) with the silicon and not aluminum atom moving away to create a vacancy may be formed.

On the basis of the discussion two possible identifications of the Si-NL10 center are proposed. According to one of them Si-NL10 center is an oxygen heat-treatment aggregate, growing in parallel to NL8 TD's and very similar to NL8 TD. However the incorporation of an acceptor would probably make it a shallow single donor instead of a double donor. An alternative explanation identifies Si-NL10 as an acceptor NL8 $(TD)^-$ state of the NL8 thermal donor. If the acceptorlike character of the Si-NL10 is further confirmed this attractive possibility will allow to understand the majority of experimental data. However in that case the core of the NL8 TD would involve a vacancy which by itself has a deep center character. Although one can expect that the presence of oxygen atoms in the direct vicinity of the vacancy would most certainly influence its electrical properties this possibility would have to be confirmed by theoretical calculations.

ACKNOWLEDGMENT

This project has been partially sponsored by the Netherlands Foundation for Fundamental Research on Matter [Stichting voor Fundamenteel Onderzoek der Materie (FOM)].

*Also at Institute of Physics, Polish Academy of Sciences, PL-02-668 Warsaw, Poland.

[1]C. S. Fuller, J. A. Ditzenberger, N. B. Hannay, and E. Buehler, Phys. Rev. **96**, 833 (1954).

[2]C. S. Fuller and R. A. Logan, J. Appl. Phys. **28**, 1427 (1957).

[3]W. Kaiser, H. L. Frisch, and H. Reiss, Phys. Rev. **112**, 1546 (1958).

[4]A. Bourret, in *Proceedings of the Thirteenth International Conference on Defects in Semiconductors, Coronado, California, 1984,* edited by L. C. Kimerling and J. M. Parsey, Jr. (The Metallurgical Society of the AIME, Warrendale, 1985), p. 129.

[5]T. Gregorkiewicz, D. A. van Wezep, H. H. P. Th. Bekman, and C. A. J. Ammerlaan, Phys. Rev. B **35**, 3810 (1987).

[6]D. Wruck and P. Gaworzewski, Phys. Status Solidi A **56**, 557 (1979).

[7]B. Pajot, H. Compain, J. Lerouille, and B. Clerjaud, Physica B + C **117&118B**, 110 (1983).

[8]S. H. Muller, M. Sprenger, E. G. Sieverts, and C. A. J. Ammerlaan, Solid State Commun. **25**, 987 (1978).

[9]S. H. Muller, E. G. Sieverts, and C. A. J. Ammerlaan, Inst. Phys. Conf. Ser. **46**, 297 (1979).

[10]K. M. Lee, J. M. Trombetta, and G. D. Watkins, in *Microscopic Identification of Electronic Defects in Semiconductors,* edited by N. M. Johnson, S. G. Bishop, and G. D. Watkins (Materials Research Society, Pittsburgh, 1985), Vol. 46, p. 263.

[11]M. Stavola, K. M. Lee, J. C. Nabity, P. E. Freeland, and L. C. Kimerling, Phys. Rev. Lett. **54**, 2639 (1985).

[12]M. Stavola and K. M. Lee, in *Oxygen, Carbon, Hydrogen and Nitrogen in Crystalline Silicon,* edited by J. C. Mikkelsen, Jr., S. J. Pearton, J. W. Corbett, and S. J. Pennycook (Materials Research Society, Pittsburg, 1986), Vol. 59, p. 95.

[13]J. W. Farmer, J. M. Meese, P. M. Henry, and C. D. Lamp, in *Proceedings of the Thirteenth International Conference on Defects in Semiconductors,* Ref. 4, p. 639.

[14]J. L. Benton, K. M. Lee, P. E. Freeland, and L. C. Kimerling, in *Proceedings of the Thirteenth International Conference on Defects in Semiconductors,* Ref. 4, p. 647.

[15]W. Kohn, in *Solid State Physics,* edited by F. Seitz and D. Turnbull (Academic, New York, 1957), Vol. 5, p. 257.

[16]L. C. Snyder and J. W. Corbett, in *Proceedings of the Thirteenth International Conference on Defects in Semiconductors,* Ref. 4, p. 693.

[17]A. Ourmazd, W. Schröter, and A. Bourret, J. Appl. Phys. **56**, 1670 (1984).

[18]R. C. Newman, J. Phys. C **18**, L967 (1985).

[19]J. Robertson and A. Ourmazd, Appl. Phys. Lett. **46**, 559

(1985).
[20]J. Michel, J. R. Niklas, J.-M. Spaeth, and C. Weinert, Phys. Rev. Lett. **57**, 611 (1986).
[21]G. G. DeLeo, C. S. Milsted, Jr., and J. C. Kralik, Phys. Rev. B **31**, 3588 (1985).
[22]H. H. P. Th. Bekman, T. Gregorkiewicz, D. A. van Wezep, and C. A. J. Ammerlaan, J. Appl. Phys. **62**, 4404 (1987).
[23]C. S. Fuller, F. H. Doleiden, and K. Wolfstirn, J. Phys. Chem. Solids **13**, 187 (1960).
[24]T. Gregorkiewicz, D. A. van Wezep, H. H. P. Th. Bekman, and C. A. J. Ammerlaan, Phys. Rev. Lett. **59**, 1702 (1987).
[25]B. Pajot (private communication).
[26]M. Sprenger, S. H. Muller, E. G. Sieverts, and C. A. J. Ammerlaan, Phys. Rev. B **35**, 1566 (1987).
[27]G. H. Fuller, J. Phys. Chem. Ref. Data **5**, 835 (1976).
[28]E. B. Hale and R. L. Mieher, Phys. Rev. **184**, 739 (1969).
[29]J. R. Morton and K. F. Preston, J. Magn. Reson. **30**, 577 (1978).
[30]R. van Kemp, Ph.D. thesis, University of Amsterdam, 1988 (unpublished).
[31]S. Canuto and A. Fazzio, Phys. Rev. B **33**, 4432 (1986).
[32]L. Pauling, *The Nature of the Chemical Bond* (Cornell University Press, Ithaca, 1960).
[33]D. R. Bosomworth, W. Hayes, A. R. L. Spray, and G. D. Watkins, Proc. R. Soc. London Ser. A **317**, 133 (1970).
[34]G. D. Watkins, in *Radiation Damage in Semiconductors* (Dunod, Paris, 1965), p. 97.
[35]H. H. P. Th. Bekman, T. Gregorkiewicz, and C. A. J. Ammerlaan, Phys. Rev. Lett. **61**, 227 (1988).